

# Scaling laws for the tropical cyclone derived from the stationary atmospheric vortex equation

Florin Spineanu and Madalina Vlad  
Association Euratom-MEC Romania  
National Institute of Laser, Plasma and Radiation Physics  
MG-36, Magurele, Bucharest, Romania

December 2, 2024

## Abstract

We present results of a numerical study of the differential equation governing the stationary states of the two-dimensional planetary atmosphere and magnetized plasma (within the Charney Hasegawa Mima model). The results show an interesting similarity with the morphology of a tropical cyclone. Quantitative comparisons are also favorable and several scaling laws can be formulated connecting the characteristic physical parameters of the tropical cyclone.

# 1 Introduction

The Charney equation describing the Rossby waves in atmosphere (Charney 1948) and the Hasegawa-Mima equation describing the drift waves in strongly magnetized plasma (Hasegawa and Mima 1978) have identical form and both exhibit an intrinsic length scale (see Horton and Hasegawa 1994). A long series of observations, experiments and theoretical (analytical and numerical) studies has established that the fluids show a natural trend to organisation. This is most obvious at relaxation from turbulent states when the fluid evolves toward a reduced subset of flow patterns, characterized by regular form of the streamfunction as shown for example by Matthaeus et. al. 1991a, Matthaeus et. al. 1991b, Kinney et al. 1995, Horton and Hasegawa 1994 (and references therein).

It has been shown (Spineanu and Vlad 2005) that the stationary states attained at late times in the evolution of the Charney-Hasegawa-Mima (CHM) fluids are described by the following equation

$$\Delta\psi + \frac{1}{2p^2} \sinh \psi (\cosh \psi - p) = 0 \quad (1)$$

(where  $p$  is a positive constant). There are confirmations that this is the equation governing the asymptotic stationary states of the CHM fluids: for Navier-Stokes fluid the scatterplots of  $(\psi, \omega) = (\text{streamfunction}, \text{vorticity})$  obtained in experiments by de Rooij et al. 1999, and the scatterplots obtained in numerical simulations by Seyler 1995 are very similar to the nonlinear term of Eq.(1).

Due to the similar analytical structure (although for largely different magnitude of parameters) of the plasma vortex and the atmospheric vortex, we expect that this equation leads to solutions that may capture the strong nonlinear character of the atmospheric vortical flows in those states where the stationarity can be assumed a good approximation. Certainly the problem of the structure of the atmospheric vortex cannot be reduced in general to only fluid nonlinear dynamics, knowing the very important role of the heat exchange and moisture transport and condensation processes. These are essential elements of tropical cyclogenesis (see Emanuel 1986 and 1989 and references therein) but it is often accepted that the fluid dynamics is an adequate framework to study the vortex structure at the late stage of the evolution (Reasor and Montgomery 2001, Kossin and Schubert 2001). The fluid dynamic nonlinearity becomes the dominant constraint determining the structure of the velocity field when the thermodynamic processes have reached the stationary equilibrium.

The objective of this work is to provide the first elements resulting from a numerical investigation of equation (1), for a range of parameters relevant for the physics of the atmosphere. The results are summarised here.

The solutions of the differential equation have the same morphology as the two-dimensional flow of a tropical cyclone (Willoughby and Black 1996, Wang and Wu 2004, Reasor and Montgomery 2001, Kossin and Schubert 2001). The solutions are characterized by a very narrow dip in the azimuthal velocity (tangential wind) in the center of the vortex. The radius of the “maximum tangential wind” or the radius of the *eye wall* is much smaller than the radius of the vortex. There is a decay of the magnitude of the azimuthal velocity toward the periphery, which is much slower compared with the fast decay toward the center. We find a very low magnitude (almost vanishing) of the vorticity over most of the vortex (approx. from the radius of maximum wind to the periphery), while the magnitude in a narrow central region is extremely high. Quantitatively, we obtain for the diameter of the cyclone’s eye a magnitude which compares well with the observations. The maximum vorticity is in a realistic range and the radial profile of the tangential velocity is similar to what is found in observations or with what is obtained in empirical models and numerical simulations. These favorable comparisons are valid in the case of mature, quasi-stationary tropical cyclones, after the phases of genesis and dynamic intensification.

In addition, the numerical study of Eq.(1) reveals the existence of metastable states (quasi-solutions) consisting of (a) extremely concentrated vortical flows, similar to the cross section of a tornado and (b) collection of vortices with symmetric positions in plane (vortex crystals).

The numerical studies carried out until now are organized in the form of several scaling relations connecting vortex characteristics to the few parameters of the Eq.(1). They may be used for comparison with observation or with more complex theoretical models.

## 2 The physical model and the field theoretical description

In this section we briefly recall the origin of Eq.(1). It is useful to consider first the ideal fluid described by the Euler equation, for which it has been shown that it evolves at relaxation toward a very ordered flow pattern, consisting of two (positive and negative) vortices. This state persists for long times, being limited by only the effect of some residual dissipation. From numerical simulations it has also been inferred the form of the flow function. It has been

found that the streamfunction  $\psi(x, y)$  obeys, in these states, the *sinh*-Poisson equation, an equation which has very special properties. It is an exactly integrable equation (by Inverse Scattering Transform) and is connected with a wide range of fundamental systems, like the Thirring lattice of spins in plane, the affine Toda system, the Gauss-Codazzi equations for embedding a surface in three dimensional space, etc. David Montgomery and his collaborators have developed a theoretical statistical model which explains the appearance of this equation in this context (Kraichnan and Montgomery 1980, Fyfe, Montgomery and Joyce 1976, Joyce and Montgomery 1973, Montgomery and Joyce 1974, Montgomery et al. 1992).

The Euler equation is

$$\left[ \frac{\partial}{\partial t} + (-\nabla_{\perp} \psi \times \hat{\mathbf{n}}) \cdot \nabla_{\perp} \right] \omega = 0 \quad (2)$$

where  $\hat{\mathbf{n}}$  is the versor perpendicular on the plane, the velocity and the vorticity are respectively  $\mathbf{v} = -\nabla_{\perp} \psi \times \hat{\mathbf{n}}$  and  $\omega = \hat{\mathbf{n}} \nabla_{\perp}^2 \psi$ . It is generally accepted (but not yet mathematically proved) that the Euler fluid may be described by an equivalent model, consisting of a set of discrete point-like vortices moving in plane under the effect of mutual interaction. The latter is expressed by a potential given by the natural logarithm of the relative distance between vortices normalized to the linear extension of the region in plane where the motion is bounded (Kraichnan and Montgomery 1980). A fundamental observation is that this formulation exhibits a particular structure: matter, field, interaction. The *matter* corresponds to the density of point-like vortices in plane; the *field* is derived from the potential and can be seen as an independent component of the system; the *interaction* appears as the usual combination of the matter current with the potential and leads to the equation of motion of the point-like vortices. The *sinh*-Poisson equation has been derived by formulating the continuum version of the point-like vortices model as a field theoretical model of interacting gauge and matter fields in the adjoint representation of  $SU(2)$  (Spineanu and Vlad 2003). The essential point of the latter derivation was the self-duality of the relaxation states of the fluid.

In its simplest form the Charney-Hasegawa-Mima equation is

$$\frac{\partial}{\partial t} (1 - \nabla_{\perp}^2) \psi - [(-\nabla_{\perp} \psi \times \hat{\mathbf{n}}) \cdot \nabla_{\perp}] \nabla_{\perp}^2 \psi = 0 \quad (3)$$

Similar to the Euler equation there is a discrete vortex model for the Charney-Hasegawa-Mima equation, where the potential of interaction is now short range (the modified Bessel function of zero order), *i.e.* it decays on the range

given by the intrinsic length of the CHM equation. This model has been used in meteorology by Morikawa (Morikawa 1960) and Stewart (Stewart 1943).

In a similar approach as for the Euler fluid, it has been developed (Spineanu and Vlad 2005) a field theoretical model for the continuous version of the point-like vortices with short range interaction, based on the Chern-Simons action for the gauge field in interaction with the nonlinear matter field, in the adjoint representation of the  $SU(2)$  algebra. In this model it is possible to derive the energy as a functional that becomes extremum on a subset of stationary states and presents particular properties. The general characterization of this family of states is their *self-duality*, which here means that the energy functional becomes minimum when the squared terms in its expression are all vanishing, leaving as lower bound for energy a quantity with topological meaning, proportional with the total vorticity.

The result is a set of equations parametrized by the solutions of the Laplace equation in two-dimensions. The Eq.(1) is the simplest of this family.

### 3 Numerical studies

To solve Eq.(1) we use the code “GIANT A software package for the numerical solution of very large systems of highly nonlinear systems” written by U. Nowak and L. Weimann (Nowak and Weiman 1990). The code is part of the numerical software library *CodeLib* of the Konrad Zuse Zentrum fur Informationstechnik Berlin. The meaning of the abbreviation is: GIANT = Global Inexact Affine Invariant Newton Techniques. This code solves nonlinear problems

$$\begin{aligned} F(\psi) &= 0 \\ \text{initial guess of solution, } \psi &= \psi^{(0)} \end{aligned} \tag{4}$$

where  $F(\psi)$  is a nonlinear partial differential operator. The integrations described here are **not** radial (*i.e.* unidimensional) which is very important since from certain initial conditions solutions consisting of multiple vortices develop. The presence of the hyperbolic trigonometric functions, with very fast variation with the argument, renders the equation difficult to solve and many initial conditions do not lead to a solution since they cannot initiate a converging iteration. With all the difficulties of finding a right initialization of the integration procedure we note however that the solution with the morphology of a tropical cyclone appears insistently from a wide class of initial functions which contains vortical flows.

### 3.1 Parameters and Initializations

Eq.(1) has been derived from the *self-duality* subset of the Euler-Lagrange variational equations for the action functional of the field-theoretical model. In this action there are only two physical parameters: the coefficient of the Chern-Simons action, which we have identified as the sound speed,  $c_s$  and the asymptotic vorticity which is the Coriolis frequency  $f_0$  (or, in plasma physics, the ion cyclotron frequency  $\Omega_{ci}$ ). The space-like parameter that normalizes the Laplace operator in the Eq.(1) is the ratio

$$\rho_g = c_s/f_0 \quad (5)$$

*i.e.* the Rossby radius  $\rho_g$  (respectively the sonic Larmor radius in plasma,  $\rho_s = c_s/\Omega_{ci}$ ). All distances implied in the solution are normalized  $\rho_g$ . The streamfunction is normalised as (the upperscript *phys* is used to indicate that the quantity is dimensional)

$$\psi = \frac{\psi^{phys}}{\rho_g^2 f_0} \quad (6)$$

The unit for the streamfunction is  $\rho_g^2 f_0$  and the unit for vorticity  $f_0$ . Then the unit for velocity is  $\rho_g f_0$ .

If we know the large radial extension of a vortex ( $L^{phys}$ ) the normalized parameter  $L$  is obtained by dividing to  $\rho_g$ . The result of integration is very sensitive to  $L$  and this points out the essential role played by  $\rho_g$  in numerical studies aiming to reproduce observations. When the depth of the atmospheric perturbation is  $H$ , the Rossby radius is  $\rho_g = (gH)^{1/2}/f_0$  (where  $g$  is the gravitational acceleration). Actually  $\rho_g$  is influenced by several other parameters than  $H$ , in particular the vorticity and it can have a range from tens to thousand kilometers. When combined with the range of vortex extensions  $L^{phys}$ , it results that  $L$  has a range between a fraction of unity to few units (in plasma  $L$  can be hundreds to thousands). For mature stationary cyclones the radial extension of the cyclon vortex and the Rossby radius are of similar magnitude and this means that we have to study the range  $L \sim 1$ .

The domain of integration is a square with a side of length  $2L$

$$(x, y) \in [-L, L] \times [-L, L] \quad (7)$$

on which we place a rectangular mesh  $n \times n$  usually with  $n = 101$ .

We impose Dirichlet boundary conditions *i.e.* the streamfunction is a constant,  $\psi_b$  on the limits of the square of integration. Here  $\psi_b$  is the smaller root of the equation  $\cosh \psi - p = 0$  and since in all our runs we have  $p = 1$ ,

the condition is  $\psi_b = 0$ . This means zero vorticity at the boundary but it has defavorable effect on the velocity field, which does not allways vanish at the border.

In general the initial profiles have been of various types: (a) symmetric profiles (*e.g.* Gaussian functions, or various annular shapes) with maximum centered on  $(0, 0)$ , or the Petviashvili-Pokhotelov vortex, Eq.(8) below; (b) functions expressed as product of trigonometric functions; or (c) collections of localised vortex-like perturbations placed randomly. In this work we report results obtained for initializations with vorticity of the same sign over all the space region. It has resulted that the monopolar vortex which may be relevant for the atmosphere physics can actually be obtained as a solution of the convergent iteration from a large class of initial conditions, of various shapes belonging to the three classes mentioned above. However, in terms of a set of parameters describing any of the classes of initialization, finding the convergence (solution) proves to be complicated and finding a solution is rather exceptional. It can be said that the regions favorable to convergence in the space of initial function are intricate and have sharp limits.

In order to simulate the formation of a vortex the main series of runs reported here have adopted as initial function (from which the iteration of GIANT starts) a monopolar, circularly symmetric form characterized by few parameters, the Petviashvili-Pokhotelov vortex

$$\psi(x, y) = \psi_0 [\sec h(kr)]^{4/3} + \psi_b. \quad (8)$$

Here  $kr = \sqrt{(x^2 + y^2)}/\delta^2$ ,  $\delta$  may be seen as a peaking factor of the initial shape,  $\psi_0$  is the amplitude and  $\psi_b$  is the boundary value. The reason to choose the form (8) is connected with the set of equation (continuity and conservation of momentum) from which the CHM equation is originally derived. It has been shown by a multiple space-time scale analysis that the late stage evolution of the full set of equation is dominated by mesoscopic scales (of the order  $\sqrt{L_n \rho_s}$  where  $L_n$  is a typical length of the gradient of the equilibrium density) where a different nonlinear mechanism is present. Instead of the nonlinearity term in (3) there is a scalar or Korteweg-DeVries nonlinearity of the type  $\psi \frac{\partial \psi}{\partial x}$  in one dimension, and the equation actually is replaced by the Flierl-Petviashvili equation (see for example Spineanu et al. 2004). Or, this equation has a solution expressed as Eq.(8). As initial function, Eq.(8) has some advantages: it has physical relevance for the system which is behind the stationary states emerging from Eq.(3); it is a vortical structure, as those which may be expected to form spontaneously in real situations; and it has few parameters which we take as coordinates in a space of initial functions that must be sampled to find solutions.

The parameters of the equation and of the initial function, which completely defines a numerical experiment, are: (a) half the length of the side of the square area taken as region of integration,  $L = L^{phys}/\rho_g$ ; (b) the constant of the equation which in these runs is taken  $p = 1$ . This implies that the boundary condition for the streamfunction, which also means zero vorticity, is  $\psi_b^{(1,2)} = \ln \left( p \pm \sqrt{p^2 - 1} \right) = 0$ ; (c) the peaking on the center, described by  $\delta$ ; (d) the amplitude of the initial function  $\psi_0$ .

The choice of an initial amplitude  $\psi_0$  favorable for reaching a solution is made easier if we use the following formula connecting the radius of the maximum azimuthal velocity  $a$  with the amplitude of the streamfunction at this maximum  $\psi_0$ :

$$a \sim \sqrt{\psi_0} \exp(-\psi_0 + 1) \quad (9)$$

This formula can be derived by simple manipulations of the equation (1), together with approximations that are made possible by some numerical experience about the orders of magnitude of the normalized quantities. It is a rather poor but useful approximation and only works for  $L \lesssim 3$ , a range which is interesting for the atmospheric vortex.

From the other types of initial profiles we briefly discuss the second one. As suggested by the numerical study of the *sinh*-Poisson equation the initial function has been taken in several runs as a product of trigonometric functions in both directions,  $x$  and  $y$ . We need to prepare the initial function in the sense that the values that are obtained for the vorticity, *i.e.* the Laplacean of the initial  $\psi$  should not be too different of what is obtained by simply inserting the initial function in the nonlinear term. The initial function is taken as

$$\psi(x, y) = \psi_0 \sin \left( k\pi \frac{x - x_{\min}}{x_{\max} - x_{\min}} \right) \sin \left( k\pi \frac{y - y_{\min}}{y_{\max} - y_{\min}} \right) \quad (10)$$

where  $x_{\min}$ ,  $x_{\max}$ ,  $y_{\min}$ ,  $y_{\max}$  are the limits of the domain Eq.(7),  $k$  is the periodicity of the profile and  $\psi_0$  is the amplitude. Eq.(10) is inserted in Eq.(1) and one requires approximative equality of the two parts, the vorticity and the nonlinearity. This is obtained by choosing a point  $(x, y)$  where the initial function is maximum and it results a condition on only the amplitude,  $\psi_0$ .

$$\Delta\psi = \psi_0 [2(k\pi)^2] \simeq \frac{1}{2} \sinh \psi_0 (\cosh \psi_0 - 1) \quad (11)$$

The equation is solved graphically and one of the roots is selected as the amplitude of the initial function. From these initializations we obtain sometimes quasi-solutions consisting of multiple vortices.



## 4 Results

### 4.1 Summary of the numerical results

The strong nonlinear character of Eq.(1) combined with the internal procedures of GIANT (with no physical significance) imprints a particular structure to a space of functions that is explored for exact solutions. The space of functions representing initial conditions are divided into disjoint parts, such that from one subset one cannot access the final configuration of another subset. This means that in order to obtain a particular type of stationary (asymptotic) solution one has to initialize in a particular subset, homotopically connected to the final state. Most of the initial conditions does not lead to convergence and possibly they correspond to turbulent physical states. Exact solutions are obtained in the form of trivial ( $\psi \equiv 0$ ) state and monopolar or multipolar vortices.

Besides exact solutions there are sets of functions that are almost solutions, *i.e.* velocity field configurations that verify the equation with only low accuracy and are normally rejected by the integration procedure at smaller tolerance. They are interesting because they appear systematically and approximately exhibit the same characteristics for a fixed  $L$ . The iteration of GIANT gets almost stuck around such a solution, which may suggest that they are metastable states of the physical fluid and eventually evolve slowly toward an exact solution, a smooth vortex. We call them quasi-solutions and we find useful to include them in our discussion.

Restricting to the case of monopolar vortices we summarize the results by saying that for every  $L$  we obtain two types of final vortices:

1. smooth, finite amplitude, vortices verifying the equation for any change in the accuracy of the integration procedure. There is a unique smooth vortex configuration for each  $L$ .
2. quasi-solutions, consisting of strongly localised vortices, with profiles for velocity and vorticity that are much narrower compared with the smooth vortices. These quasi-solutions are persistently obtained and it seems that there is only one configuration for each  $L$ .

### 4.2 Solutions with the morphology of *tropical cyclones*

We are focusing here on the type of solutions that exhibit strong similarities with the morphology of a horizontal cross section of a tropical cyclone. These are circular symmetric solutions with a strong maximum of the tangential velocity, strong concentration of vorticity.

Taking for illustration the smooth vortex obtained for  $L = 1.25$  we note that the solution has cylindrical symmetry around the center. Fig.1 presents a section of the streamfunction  $\psi(x, y)$  along the diagonal of the domain  $(x, y)$ . A section of the vorticity  $\omega(x, y)$  is presented in Fig.2.

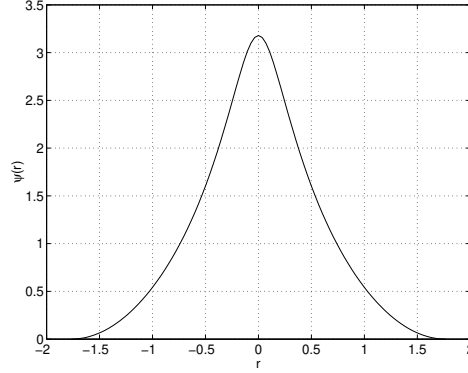


Figure 1: Solution  $\psi(x, y)$  along the diagonal of the square, for the smooth vortex at  $L = 1.25$ .

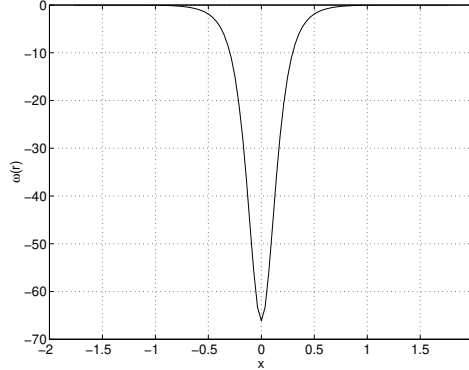


Figure 2: Vorticity calculated from  $\psi(x, y)$  obtained by integration.

In order to quantify the accuracy of integration we collect in all the domain  $(x, y)$  the pairs  $(\psi, \omega)$  and plot them together with the line representing the nonlinear term in Eq.(1), Fig.3. The scatterplot of  $(\psi, \omega)$  is almost superposed on this line. The scatterplot of the pairs  $[\omega, -\frac{1}{2} \sinh \psi (\cosh \psi - 1)]$  (not shown) indicates a close clustering around the diagonal. Other tests are possible and they show that the integration is very good on most of the region and good within the imposed accuracy in the regions where the second derivative is very high.

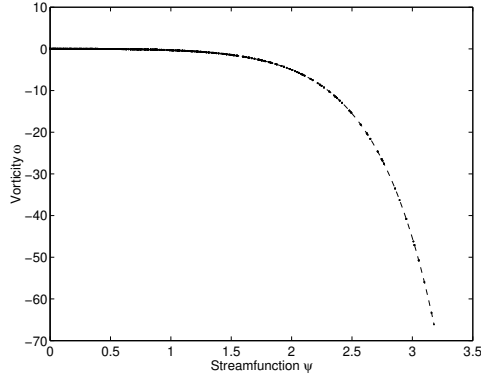


Figure 3: Scatterplot  $(\psi, \omega)$ , for the smooth vortex at  $L = 1.25$ .

The tangential component of the velocity is shown in Fig.4. The narrow dip in the center is clearly visible and its radial extension can be compared with the extension of the whole domain.

We have plotted in Fig.5 the section along the diagonal of the amplitude of the azimuthal component of the velocity.

In general the radial component of the velocity is much smaller than the azimuthal component. For this example ( $L = 1.25$ ) is in a ratio  $|v_r| / |v_\theta| \sim 0.4/4 = 1/10$  and integrated over a circle shows no net inflow to the axis.

The large amount of results for the range of  $L : 0 < L \leq 10$ , allows to formulate two remarks. First we note that for larger  $L$  the profile of the azimuthal velocity shows smaller amplitude and larger radius of the circle of maximum velocity. Second, this variation with  $L$  is much faster for low  $L$  (less or comparable to 1). The differences in the quantitative characteristics of the vortices for even small variation of  $L$  in this range are substantial. Below we provide a scaling which shows exponential behavior, Eq.(12).

### 4.3 Quasi-solutions : strongly localised vortices

For comparison we present the profiles of the solution  $\psi(x, y)$  Fig.6, vorticity  $\omega(x, y)$  Fig.7 and azimuthal velocity  $v_\theta(x, y)$  Fig.8 for the quasi-solution that corresponds to the same  $L = 1.25$ . The sections are along the diagonal, denoted  $r$ . One should note that the total vorticity (obtained by integrating over the square) is however smaller than that for the corresponding smooth vortex shown in the preceding figures. The total energy  $E = (2L)^{-2} \int d^2r (v^2/2)$  for a fluid density  $\rho_0 \equiv 1$ , is larger for the concentrated vortices compared to the smooth ones.

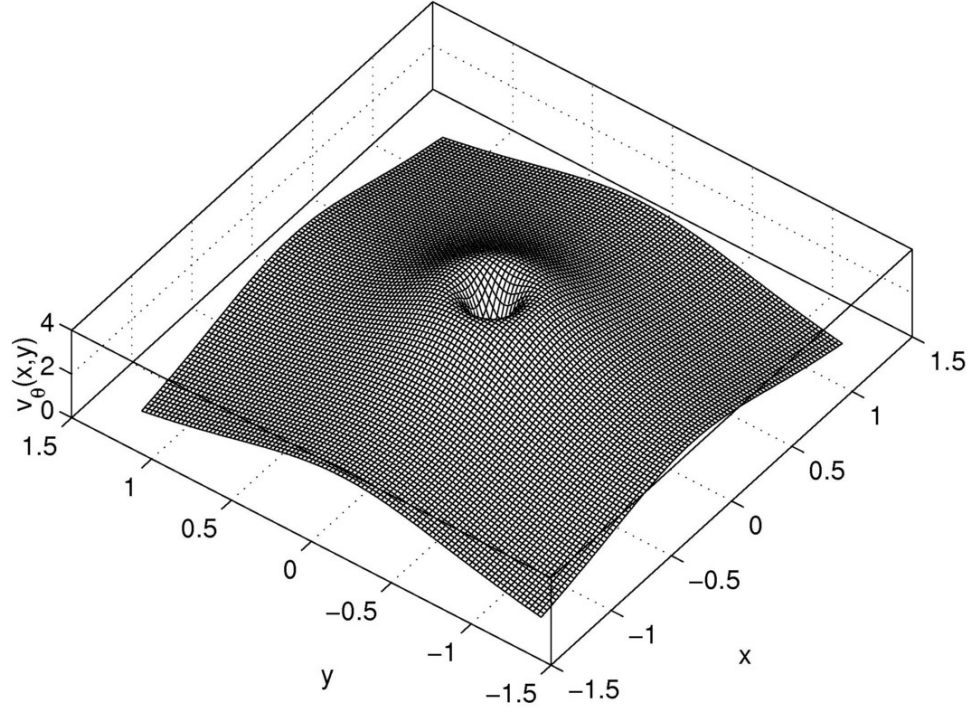


Figure 4: Azimuthal velocity  $v_\theta(x,y)$  for the smooth vortex at  $L = 1.25$ .

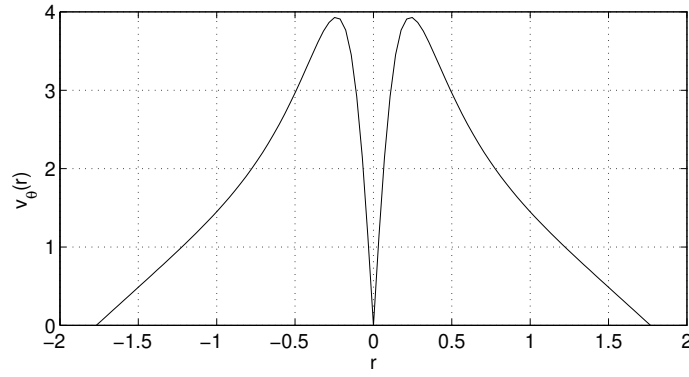


Figure 5: Azimuthal velocity  $v_\theta(x,y)$  along the diagonal of the square of integration, for the smooth vortex at  $L = 1.25$ .

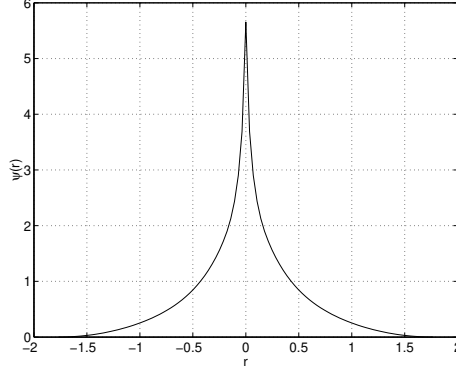


Figure 6: Streamfunction  $\psi(x, y)$  along the diagonal of the square of integration, for the quasi-solution at  $L = 1.25$ .

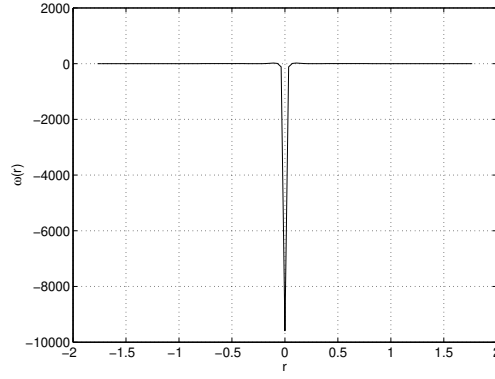


Figure 7: Vorticity  $\omega(x, y)$  along the diagonal of the square of integration, for the quasi-solution at  $L = 1.25$ .

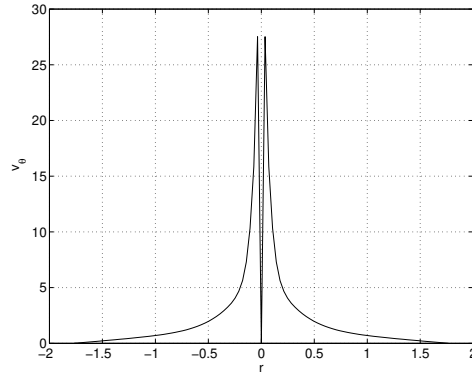


Figure 8: Azimuthal velocity  $v_\theta(x, y)$  along the diagonal of the square of integration, for the quasi-solution at  $L = 1.25$ .

#### 4.4 Quasi-solutions : multiple vortices

There are episodic structures of multiple vortices that are detected as solutions under a certain precision and which however evolve to symmetric monopolar vortex when the system is allowed to run further, under a higher precision.

It is worth to mention that in a numerical experiment we have identified a state where two vortices have been formed, placed in symmetrical positions along the diagonal of the square domain  $L = 0.5$ . The initial function is trigonometric with  $k = 2$  in Eq.(10) with a coefficient  $\psi_0 = 3.8$ . Examining this structure with higher precision, after a longer iteration sequence the final solution was again the centered smooth vortex known for  $L = 0.5$ . Therefore from the point of view of the numerical experience this state of two vortices is irrelevant. However, the persistence of this state inside the iterative search may indicate that it is close to a solution, possibly less structurally stable.

Four vortices have been obtained in a run starting from trigonometric initial function. The initial function is trigonometric Eq.(10) with  $k = 3$ . The results show the formation of four vortices, as shown by Fig.9. Each of them has a structure that is similar to the one presented in Fig.1. It is interesting to note that again the vorticity is almost zero everywhere on the domain, except the regions of the four vortices, where it reaches very high values. The local tangential velocity presents the same very fast decay to the center of the vortex and each vortex is similar in structure with a typical cyclone.

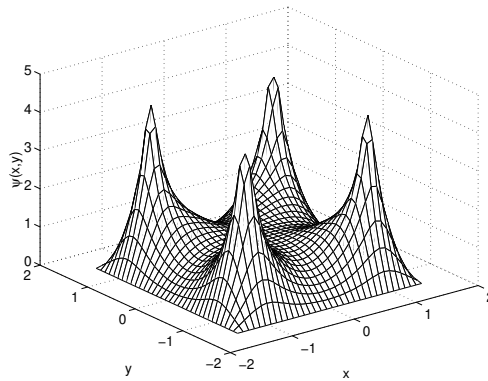


Figure 9: The scalar streamfunction  $\psi(x, y)$  for a four-vortices solution.

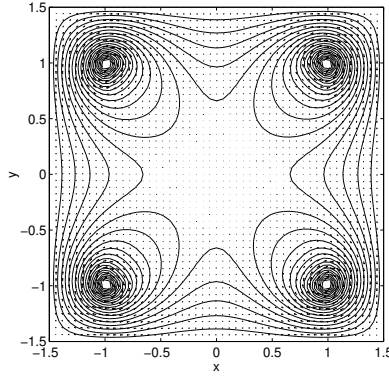


Figure 10: The contours of the scalar streamfunction  $\psi(x, y)$  and the vector field  $(v_x, v_y)$  for a four-vortices solution.

## 5 Scaling laws inferred from numerical results

As mentioned before the nontrivial results of monopolar vortices are systematically of two types: a smooth vortex solution and a strongly localised quasi-solution. These are always the same for a fixed  $L$ . Their characteristics strongly depends on  $L$ , especially for the lower part of the range, where  $L$  is few units or less.

Since the monopolar final states are independent of the initial conditions from which we start and of the particular numerical method of solution (GI-ANT) the scaling relations between the characteristics of the final vortices are objective and reflect properties of the equation itself. In addition the results (smooth vortex and narrow quasi-solution) are unique for a particular  $L$ , suggesting we can collect all numerical results in a form of nomograms or analytic (eventually spline functions) fit. However, we will look instead for analytic formulas which, even approximative, are simpler to use. We examine (a) the scaling of the *maximum tangential velocity* with the length of the space domain,  $L$ ; (b) the scaling of the *radius of the eye-wall* of the atmospheric vortex with the length  $L$ . Finally we will examine the existence of a linear relation between *the energy and the vorticity* in the final states.

## 5.1 The scaling of the maximal tangential velocity with the extension of the atmospheric vortex

We have inferred from numerical data an expression showing variation of  $v_{\theta}^{\max}$

$$v_{\theta}^{\max}(L) \simeq \frac{e^2}{2} \left[ \alpha \exp\left(\frac{1}{L}\right) - 1 \right] \quad (12)$$

for the interval  $0 < L < 6$ .

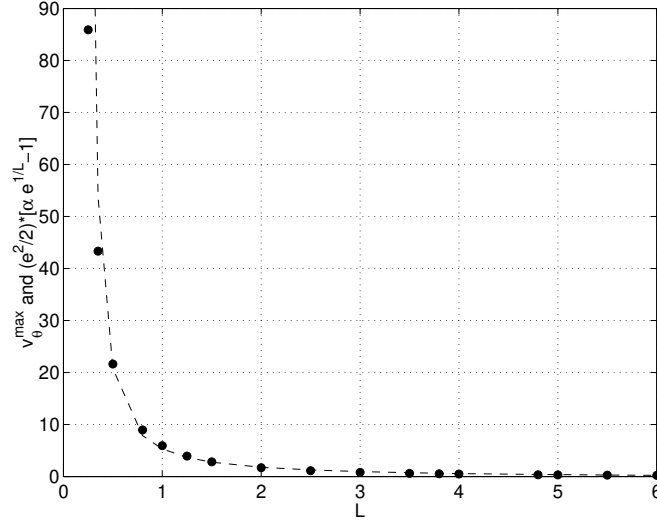


Figure 11: The maximum tangential velocity  $v_{\theta}^{\max}$  as function of  $L$ . The dashed line represents the fit according to Eq.(12)

For  $\alpha = 0.97$  this scaling works better for  $L$  around 1, and is a poor approximation over the range less than 0.4. At  $L \gtrsim 1.5$  this formula overestimates the maximum velocity and will not be used when we dispose, for the particular  $L$ , of the full numerical set as obtained by GIANT. However many observational data fall in the range  $L \sim 1$  where Eq.(12) is a good fit and there it may be useful for a rapid estimation.

## 5.2 The scaling of the radius of the eye-wall with the extension of the atmospheric vortex

On the basis of many runs we have tried to infer a possible relation between the radius of the *eyewall*, (the radius of the circle where the tangential velocity is maximum) and the parameter  $L$ .



When the data collected for a larger range of  $L$ ,  $0 < L \leq 6$ , is taken into account, it appears that there is an approximative linear dependence of  $r_{v_\theta}^{max}(L)$  on  $L$ .

$$r_{v_\theta}^{max}(L) = 0.11 \left( -\frac{1}{2} + L \right) \quad (13)$$

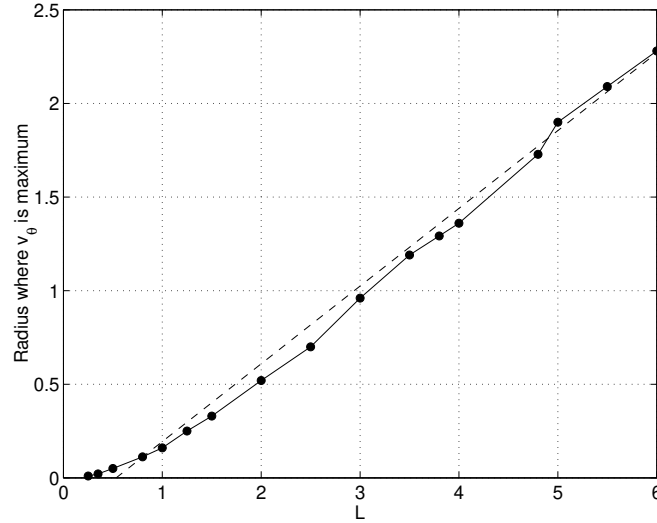


Figure 12: The radial position where the tangential velocity  $v_\theta^{max}$  attains its maximum, as function of  $L$ . The dashed line represents the linear fit according to Eq.(13)

As can be seen from Fig.12 this linear fit is too approximative and in particular does not work well for low  $L$ ,  $0 < L \lesssim 2.5$ . Or this is the range that is relevant for the atmospheric vortex. It is necessary to look for a different fit for that range.

In our rectangular geometry it seems more appropriate to take as a spatial extension (instead of  $L$ ) the distance from the center where the velocity is zero, *i.e.* half the diagonal of the domain of integration

$$R_{max} \sim \sqrt{2}L \quad (14)$$

and to normalize the eye-wall radius to this distance. Then the same numerical information can be organized to show the dependence of  $r_{v_\theta}^{max}/R_{max}$  on the length  $L$ . The following simple function offers a satisfactory fit for the low  $L$  range

$$\frac{r_{v_\theta}^{max}}{R_{max}} = \frac{1}{4} \left[ 1 - \exp \left( -\frac{R_{max}}{2} \right) \right] \quad (15)$$

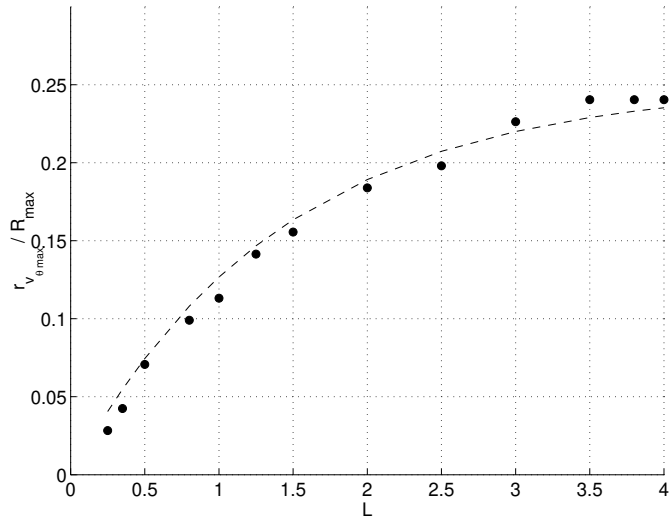


Figure 13: Ratio of the radius where maximum of  $v_\theta$  is attained to the radius of the maximum extension of the vortex,  $R_{\max}$  represented as function of the length  $L$ . The dashed line is the fit according to Eq.(15).

Although it slightly overestimates the ratio (see Fig.13), this formula is practical by its simplicity and may be used for estimations based on observational data, as will be described later.

### 5.3 Energy and vorticity in the final states

The smooth and respectively the concentrated vortices are persistently obtained, from a wide variety of initial conditions. This suggests that, apart variations due to the accuracy of the iteration process, these states really represent a stationary state and respectively a quasi-stationary state of the fluid. Their characteristics are completely determined once we have fixed the spatial extension of the domain, the length  $L$ , which is half the side of the square on which the integration is performed, with  $\psi = 0$  on its boundaries.

In particular the final states for a fixed  $L$  are characterised by two quantities, the total final energy and the total final vorticity and there are two pairs  $(E_{fin}, \Omega_{fin})$ : one for the smooth vortex and one for the narrow vortex. When these pairs are collected from all numerical experiences for a particular  $L$ , the precision of numerical determination of the solution is reflected in the dispersion of the points around an average one which may be supposed to be the exact solution. For the smooth vortices the dispersion is insignifiant, confirming that the numerical identification of this solution is very good, for

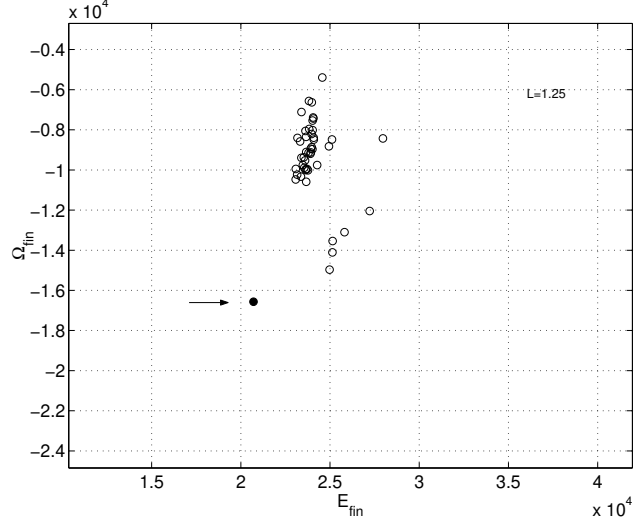


Figure 14: Energy and vorticity in the final states obtained at  $L = 1.25$ . The dot indicated by the arrow consists of 84 smooth vortices, while the 46 narrow vortices (open circles) show a dispersion in energy and vorticity.

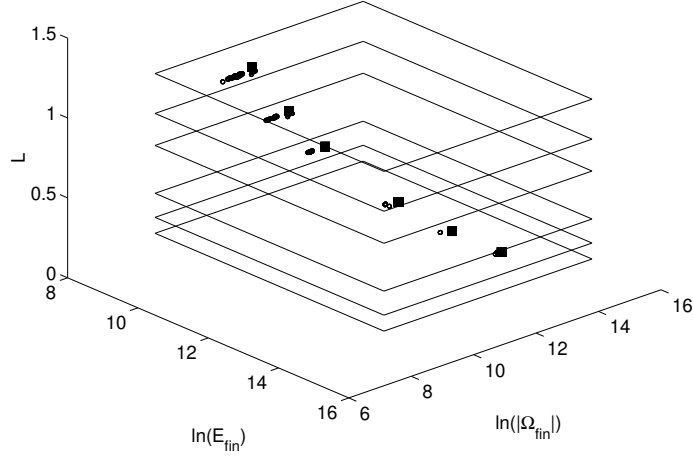


Figure 15: Energy and vorticity in the final states for several low  $L$  values. The smooth (black squares) and concentrated vortices (small circles) are plotted in logarithmic scale. Every plane corresponds to a particular  $L$  value: 0.25, 0.35, 0.5, 0.8 and 1.25.

all initializations. For the strongly localized vortex the dispersion is apparent and is connected with the higher magnitude of the second derivative on a very small area. However the results are clearly clustered around an average value which one can use to study various scaling relations. This difference is exemplified in Fig.14 showing 130 results for  $L = 1.25$ , both smooth and narrow vortices. The black dot indicated by the arrow actually consists of 84 distinct dots representing almost identical results for the smooth vortex at  $L = 1.25$ . The open circles are 46 quasi-solutions narrow vortices, which have very close characteristics ( $v_\theta(x, y)$ ,  $r_{v_\theta}^{\max}$ , etc.). They clearly represent approximations of a unique quasi-solution. The dispersion in the final energy and vorticity are a consequence of differences in the calculated second derivative of  $\psi$  on a very small area, the reason for which they are actually rejected by GIANT. In Fig.15) data are plotted for several values of  $L$ .

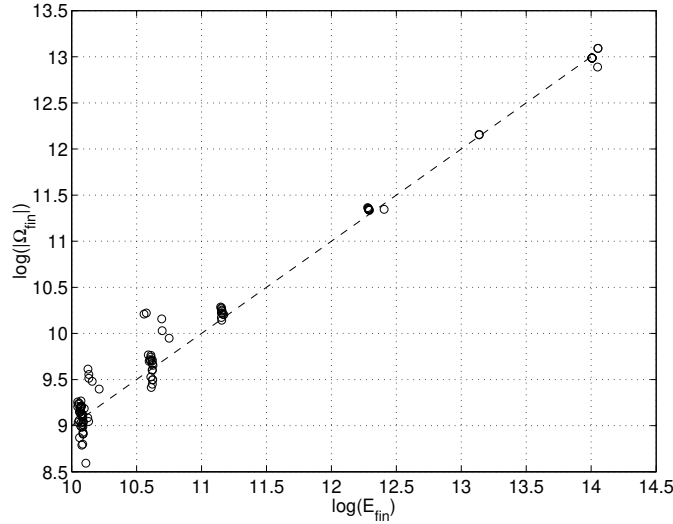


Figure 16: Energy and vorticity in the final states corresponding to strongly localized vortices are plotted in logarithmic scale,  $(\ln(E_{fin}), \ln(|\Omega_{fin}|))$ . The dashed line has slope 1 which means that  $E_{fin}$  is proportional to  $\Omega_{fin}$ .

The first important relation is between the energy  $E_{fin}$  and the vorticity  $\Omega_{fin}$  in the final states. The field theoretical model from which the equation is derived points out the existence of a lower bound for the energy functional for the point-like vortices: the energy is expressed as a sum of squared terms plus a supplementary term that has a topological content. The minimum of the energy is obtained by taking the squared terms to zero (and this leads to the self-dual equations and further to Eq.(1)) and this makes the energy equal to the topological term. Integrating on all plane this equality takes

the form of a proportionality of the total energy and the total vorticity in the fluid motion. Therefore the numerical results collected for all  $L$  should exhibit a linear relationship between  $E_{fin}$  and  $\Omega_{fin}$ . Now we have for each  $L$  two pairs  $(E_{fin}, \Omega_{fin})$  and we can try to verify this linear relations for both. The total vorticity can be calculated easily in both cases, since the vorticity has a very good spatial limitation around the eye and decays rapidly to zero. The total energy is calculated by integrating the squared velocity but the square domain of integration actually does not have everywhere zero velocity at the boundary, especially for higher  $L$ . Then a certain amount of energy cannot be included and  $E_{fin}$  is not reliable. This is the case with almost all smooth vortices (except possibly the very small  $L \sim 0.25 \dots 0.5$ , where the localization of the smooth vortex is more pronounced). However, for the strongly localized vortices this problem does not arise, for any  $L$ . Fig.16 shows that there is indeed a linear relation between the energy and the vorticity. It is visible from this log-log plot of the pairs, where the dashed line has slope 1.

With the reserves that have been formulated above, one can still look for a possible relation between the final energy and vorticity in the case of smooth vortices as results from the numerical integration. For the range of  $L$  up to 6 Fig.17 shows the data of the smooth vortices in log-log scale.

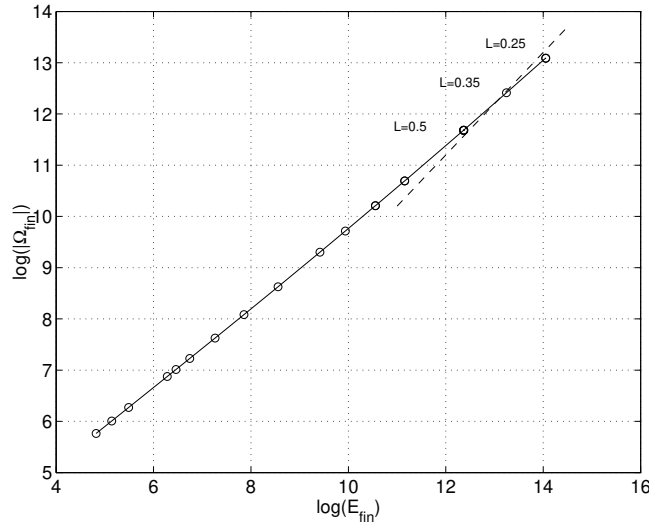


Figure 17: Energy and vorticity in the final states are plotted in logarithmic scale,  $(\ln(E_{fin}), \ln(|\Omega_{fin}|))$ . The dashed line is a linear dependence as in Eq.(16)

For low values  $L \leq 0.5$  (where the velocity approaches zero on the bound-

aries and the calculated energy is closer to the total energy) data are not far from a linear relation

$$E_{fin} \simeq \text{const} \times \Omega_{fin} \quad (16)$$

At high values,  $L > 2.5$ , the following scaling provides a better approximation.

$$\frac{E_{fin}L^2}{\Omega_{fin}} = -1 + 2.5L \quad (17)$$

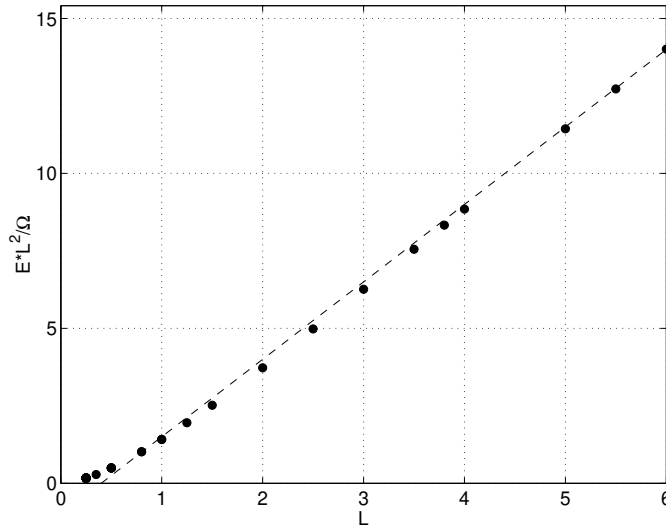


Figure 18: For the final states the pair of values  $E_{fin}, \Omega_{fin}$  are combined in the quantity  $E_{fin}L^2/\Omega_{fin}$  and this is represented as function of  $L$ . The dashed line represents the fit with the linear function Eq.(17).

This is represented in Fig.18. The fact that it refers to velocity profiles that are clipped by the square of integration limits the usefulness of this formula.

#### 5.4 The existence of a threshold in the initial energy and vorticity for obtaining a solution

Numerical simulations of basic fluid equations have shown that there is a boundary in the space of the initial configurations which separates two kinds of behaviors: on one side there are states from which the fluid evolves to random, turbulent states and on the other side there are initial configurations

giving in long run organised, highly ordered flow with a vortical pattern. In the case of the Navier-Stokes equation this limit has been called the *ergodic boundary* by Deem and Zabusky (1971). In our case there is no time evolution and the iterations of GIANT have no particular physical meaning. We simply note however that a similar separation occurs in the present case. For any fixed  $L$  the iteration of GIANT converges to a smooth vortex only if the amplitude of the initial function  $\psi_0$  is higher than a particular value, depending on the peaking parameter  $\delta$ . This can be translated into a condition for the initial energy and vorticity. Choosing  $L = 0.5$  we have represented in Fig.19 the points  $(E_{ini}, \Omega_{ini})$  corresponding to all types of final results: zero (asterisk), smooth vortex (open circles), narrow quasi-solution (black dots).

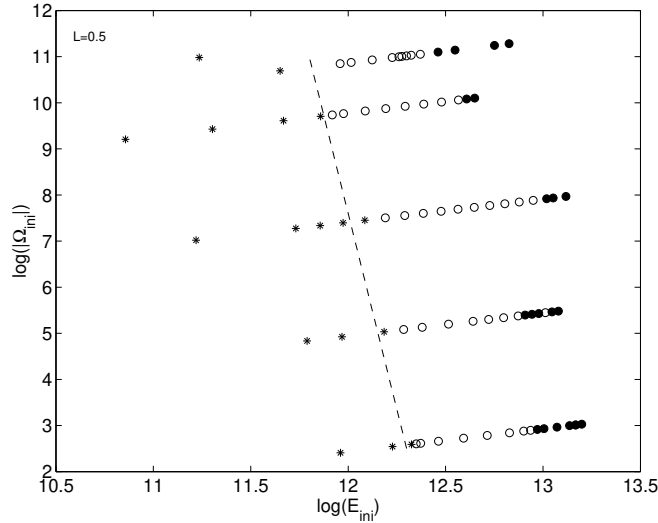


Figure 19: Set of points in the plane  $(E_{ini}, \Omega_{ini})$  from which the integrations for  $L = 0.5$  have been started, with the initial form Eq.(8). The points are distinguished according to the final states: (1) asterisks are initializations leading to trivial, zero, final state; (2) open circles are initializations leading to smooth vortex solutions; (3) black circles are initializations leading to quasi-solutions with very narrow vorticity. The dashed line is a tentative separation of the trivial solutions (at left) from the smooth vortices (at right). To the right of the rightmost black circles there is no solution.

For purely orientative purpose a line is drawn, which approximately separates initial states leading to trivial solution  $\psi \equiv 0$  (at left) from the initial states leading to smooth vortices (at right). This is almost vertical,  $\Omega_{ini} - \Omega_{ini}^0 \sim (E_{ini} - E_{ini}^0)^{-17}$  with  $(E_{ini}^0, \Omega_{ini}^0)$  one of the points on the limit.

## 6 Practical application of the scaling laws

In this section we discuss how to use the scaling relations we have derived when we want to compare with a real observational data of a tropical cyclone. Since for a fixed  $L$  the integration provides a unique smooth vortex, all data regarding this vortex are available in the form of functions :  $\psi(x, y)$ ,  $\omega(x, y)$ ,  $v_\theta(x, y)$ , and derived quantities :  $r_{v_\theta}^{\max}$ ,  $v_\theta^{\max}$ ,  $E_{fin}$ ,  $\Omega_{fin}$ . All are *normalized* and the first task is to identify the physical units that will relate these quantities to the physical data. Basically there are two units:  $\rho_g$  and  $f_0$  and the latter is assumed known.

A possible starting point is to estimate (from observations) the ratio between the radius of the circle of maximum azimuthal velocity  $r_{v_\theta}^{phys}$  and the radius of the minimum disc containing the cyclone,  $R_{\max}^{phys}$  (here as usual the upperscript *phys* means that the quantities are dimensional). Suppose this ratio can be estimated on the basis of a satellite picture. Then we can use Eq.(15) or Fig.13 to identify the parameter  $L$ . Since a real-life observation provides also the physical radius of the cyclone,  $R_{\max}^{phys}$  we can determine the Rossby radius from:  $R_{\max}^{phys} = \sqrt{2}L^{phys} = \sqrt{2}\rho_g L$  where we use  $L$  as determined. Then the unit of the physical quantities are calculated :  $\rho_g f_0$  for velocity and  $\rho_g^2 f_0$  for the streamfunction. From the runs of the code for  $L$  we dispose of profiles for all (normalized) variables. Using the units we can calculate some characteristics that can be further compared with the observations: the maximum azimuthal velocity  $v_{\max}^{phys}$ , the profile of the velocity, the vorticity, etc.

### 6.1 Example 1

We use pictures of the profile of the mean tangential wind for the hurricane Andrew, according to Willoughby and Black 1996. In Fig.3b of this reference it is represented the west to east wind profile before the eyewall replacement (23 August 1665 UTC). We retrieve the approximate values:  $v_{\theta \max}^{phys} \simeq 68$  (m/s),  $r_{v_\theta}^{phys} \simeq 12$  (km) and we assume (with a certain extension beyond the limits presented in the figure)  $R_{\max}^{phys} \simeq 120$  (km). From this we calculate

$$\frac{r_{v_\theta}^{phys}}{R_{\max}^{phys}} \simeq \frac{12}{120} = 0.1 \quad (18)$$

With this value we turn to Eq.(15) to calculate  $R_{\max}$  and then  $L$ .

$$\frac{1}{4} \left[ 1 - \exp \left( -\frac{R_{\max}}{2} \right) \right] = \frac{r_{v_\theta}^{\max}}{R_{\max}} = \frac{r_{v_\theta}^{phys}}{R_{\max}^{phys}} = 0.1 \quad (19)$$



with the result

$$R_{\max} \simeq 1.0217, \quad L \simeq 0.72 \quad (20)$$

Taking  $L = 0.72$ , we have at this moment at our disposal all the set of results that are obtained numerically for the smooth vortex at this  $L$ . Coming back to the physical data we now use the spatial extension of the vortex,  $R_{\max}^{phys} \simeq 120$  (km) to calculate the Rossby radius  $\rho_g$ , *i.e.* the space normalization

$$\rho_g = \frac{R_{\max}^{phys}}{\sqrt{2}L} = \frac{120}{\sqrt{20.72}} \simeq 117.85 \text{ (km)}$$

Now we can calculate the other physical units:  $\bar{\omega} = f_0 = 5 \times 10^{-5}$  ( $s^{-1}$ ) (from Emanuel 1989, Table 1), for velocity  $\rho_g f_0 = 5.9$  (m/s), for streamfunction  $\rho_g^2 f_0 = 0.694 \times 10^6$  ( $m^2/s$ ). From the set  $L = 0.72$  we find  $v_{\theta}^{\max} = 10.9$ . Note that the Eq.(12) gives a close value: 10.67. The physical value results  $v_{\theta}^{\max} = 64.31$  (m/s). This is comparable to 68 (m/s) the value shown in the mentioned reference. The maximum vorticity is  $|\omega_{\max}| = 491.2 \times f_0 = 0.0246$  ( $s^{-1}$ ).

## 6.2 Example 2

For this example we adopt the following input data: the ratio of the full spatial extension of the hurricane to the radius of maximum tangential wind is  $R_{\max}^{phys}/r_{v_{\theta}^{\max}}^{phys} \sim 9$ ; and the physical extension of the hurricane is  $R_{\max}^{phys} \sim 300$  (km). The data can be compared with the picture taken by NASA at 28 August 2005, when the hurricane Katrina was above the Mexic gulf, but the identification of reliable physical data is problematic in our simple approach. Eq.(15) is used to find

$$L \sim \frac{1}{\sqrt{2}} (-2) \ln \left( 1 - 4 \frac{r_{v_{\theta}^{\max}}^{phys}}{R_{\max}^{phys}} \right) = 0.8313$$

It results the Rossby radius  $\rho_g = R_{\max}^{phys}/(\sqrt{2}L) \sim 212$  (km). The unit of vorticity is the Coriolis parameter  $\bar{\omega} = f_0 = 5 \times 10^{-5}$  ( $s^{-1}$ ) and we have the unit of velocity  $\bar{v} = \rho_g \bar{\omega} = 10.6$  (m/s). Looking again to the results from the numerical integration for  $L = 0.83$  we find the magnitude of the normalized tangential velocity  $v_{\theta}^{\max} = 8.37$  (note that Eq.(12) gives a similar value, 8.26), which means that in physical units we have

$$v_{\theta}^{phys} \sim 88.6 \text{ (m/s)}$$

This gives a very high value for the maximum tangential wind, but the range is still realistic. The maximum vorticity is  $|\omega_{\max}| = 290.38 \times f_0 = 0.0145$  ( $s^{-1}$ ).

### 6.3 Example 3

Since we admit there is a significant arbitrariness in the identification of the input data, we *choose* for the third example the approximative value  $R_{\max}^{phys}/r_{v_{\theta}^{\max}}^{phys} \sim 8$  and a radius of maximum extension of the hurricane of  $R_{\max}^{phys} \sim 350$  (km). (We can say that this is only inspired by the picture taken by NASA on the hurricane Rita, September 21, 2005). From this data it is obtained

$$L \sim \frac{1}{\sqrt{2}} (-2) \ln \left( 1 - 4 \frac{r_{v_{\theta}^{\max}}^{phys}}{R_{\max}^{phys}} \right) = 0.9803$$

Then we can calculate the Rossby radius  $\rho_g = R_{\max}^{phys}/(\sqrt{2}L) = 252.47$  (km). Taking the Coriolis parameter  $f_0 = 5 \times 10^{-5}$  ( $s^{-1}$ ) we have the physical unit of velocity  $\bar{v} = \rho_g \bar{\omega} = 12.6$  (m/s). The maximum tangential velocity for  $L = 0.98$  can be calculated using the scaling formula Eq.(12), with the result  $v_{\theta}^{\max} = 6.24$ . We will use however the exact result, provided by numerical integration with GIANT of Eq.(1),  $v_{\theta}^{\max} = 6.15$  and this leads to the physical velocity

$$v_{\theta \max}^{phys} = 77.5 \text{ (m/s)}$$

The maximum vorticity is  $|\omega_{\max}| = 158.34 \times f_0 = 0.0079$  ( $s^{-1}$ ).

From these examples we conclude that the results of the estimations can be significantly affected by the approximations on the observational data, especially that of the ratio  $r_{v_{\theta}^{\max}}/R_{\max}$ . This is because the magnitude of  $L$  which is obtained from Eq.(15) using a reasonable input value for this ratio belongs to a range where the variations with  $L$  of all the characteristics of the solution ( $\psi$ ,  $\omega$ ,  $v_{\theta}$ ,  $r_{v_{\theta}^{\max}}$ ) are substantial. It is sufficient to look at the dependence of  $v_{\theta}^{\max}$  on  $L$ , Fig.11.

## 7 Discussion

At the origin of our approach it is the Charney-Hasegawa-Mima model, a two-dimensional, nondissipative and purely fluid-dynamical (no thermal process) model. Although is a simplified model it exhibits (via the field-theoretical formulation) a compact analytic and algebraic structure, self-duality, leading to Eq.(1). We have several arguments in favor of the conclusion that Eq.(1) may represent the fluid nonlinear-dynamic part of the atmospheric vortex. First, the profiles obtained by solving Eq.(1) are similar to results already known (from observations or numerical simulation) for the same quantities.

1. The profile of the the tangential velocity, our Fig.5, is similar to typical tropical cyclone velocity profiles, as represented in Fig.2 of Wang and Wu 2004. This is also confirmed by close similarity with the Fig.1a from Reasor and Montgomery 2001 and with the profile given by the Holland model or with the experimental observation (for Andrew hurricane, Willoughby and Black 1996).
2. The fast decay to zero of the vorticity  $\omega$  shown in our Fig.2 is similar to what is shown in Fig.1a of Kossin and Schubert 2001; ideally (without dissipation and friction) for mature hurricanes the maximum of  $\omega$  is on the center.
3. We note that in a series of reported numerical simulations, the tendency of the fields is to evolve toward profiles that are very close to those shown in our figures 2 and 5. For example, the Fig.7a and 7b of Kossin and Schubert 2001 show the evolution of the vorticity and mean of the tangential velocity from initial profiles which correspond to a narrow ring of vorticity to profiles that show clear resemblance with our figures 2 and 5. The same striking evolution to profiles similar to ours appears in Figs.7 a and b of the same Reference. We have investigated whether a radially annular profile of vorticity can be a solution of our equation (1). The result is negative, which may explain why such an initial profile evolves to either a set of vortices (vortex-crystal) or to a centrally peaked structure as in Fig.2.

Second, we obtain a good consistency between our quantitative results for an atmospheric vortex (using approximative input information) and the values measured or obtained in numerical simulations.

Finally, the quasi-solutions which appear to be an interesting feature of this equation, are compatible with a series of previously known results: the four vortices represented in our figure 10 are similar to the Figure 4a from the work of Kossin and Schubert 2001. And the evolution to a monopolar structure we obtain is similar to the same process reported in this reference.

The numerical results have made possible to formulate several scaling relations connecting parameters of the atmospheric vortex. These are simple formulas, intended for practical use, inevitably approximative and contain a certain amount of arbitrariness. This is because our purpose was to infer an analytical expression for a curve which is determined numerically (or: is known in the form of a simple table of values). Other expressions are possible and are worth to look for. A true scaling law will become possible only as a result of an *analytical* investigation of the properties of the equation. On

the other hand, this equation does not have a Backlund transform and is probable not integrable the Inverse Scattering Transform.

An important field of future investigation (analytical and numerical) is represented by the *quasi-solutions*, elements of a space of functions that apparently come very close of verifying the equation. Are they close to the extremum of the action functional of the full field-theoretical model, for example, are they metastable states? From the physical point of view it may result that these states can be rendered more stable by processes that are connected with what is missing from the Charney-Hasegawa-Mima model: third dimension, viscosity, thermal processes. It is worth to examine the role of the strongly localized quasi-solutions in models of tornadoes.

Developing from the present one, a future self-consistent model will have to include variation of the Rossby radius with the dynamical properties of the vortex. Since this implies to consider that the coefficient of the Chern-Simons part in the Lagrangian is a nonlinear function of the scalar field, it is difficult to say if the self-duality will be maintained.

The investigation of this equation, and, most important, of the field-theoretical model from which it is derived, are worth to be continued.

**Acknowledgments.** We are grateful to Professor David Montgomery for many interesting discussions. The hospitality of Professor S.-I. Itoh and of Professor M. Yagi at the Kyushu University is gratefully acknowledged.

This work has been partly supported by a grant from the Japan Society for the Promotion of Science.

## References

- |                            |  |
|----------------------------|--|
| [Charney 1948]             | Charney, J. G., 1948: Geophys. Public. Kosjones Nors. Videnshap. Akad. Oslo, <b>17</b> , 3.  |
| [Hasegawa and Mima 1978]   | Hasegawa, A. and K. Mima, 1978: Pseudo-three-dimensional states in magnetized nonuniform plasmas, <i>Phys. Fluids</i> <b>21</b> , 87-92. |
| [Horton and Hasegawa 1994] | Horton, W. and A. Hasegawa, 1994: Quasi-two-dimensional dynamics of plasmas and fluids, <i>Chaos</i> <b>4</b> , 227-251.                 |

- [Matthaeus et al. 1991a] Matthaeus, W.H., W.T. Stribling, D. Martinez, S. Oughton and D. Montgomery, 1991: Selective decay and coherent vortices in two-dimensional incompressible turbulence, *Phys. Rev. Lett.* **66**, 2731-2734.
- [Matthaeus et al. 1991b] Matthaeus, W.H., W.T. Stribling, D. Martinez, S. Oughton and D. Montgomery, 1991: Decaying, two-dimensional, Navier-Stokes turbulence at very long times, *Physica* **D51**, 531-538.
- [Kinney et al. 2005] Kinney, R., J. C. McWilliams and T. Tajima, 1995: Coherent structures and turbulent cascades in two-dimensional incompressible magnetohydrodynamic turbulence, *Phys. Plasmas* **2**, 3623-3639.
- [Spineanu and Vlad 2005] Spineanu, F. and M. Vlad, 2005: Stationary vortical flows in two-dimensional plasma and planetary atmospheres, *Phys.Rev.Lett* **94**, 235003-1-4.
- [de Rooij et al. 1999] de Rooij, F., P. F. Linden and S. B. Dalziel, 1999: Experimental investigations of quasi-two-dimensional vortices in a stratified fluid with source-sink forcing, *J. Fluid Mech.* **383**, 249-283.
- [Seyler 1996] Seyler, C.E., 1996: On the most probable states of two-dimensional plasma, *J. Plasma Physics* **56**, 553-567.
- [Emanuel 1986] Emanuel, K.A., 1986: An air-sea interaction theory for tropical cyclones. Part I. *J. Atmos. Sci.* **43**, 585-604.
- [Emanuel 1989] Emanuel, K.A., 1989: The finite-amplitude nature of tropical cyclogenesis, *J. Atmos. Sci.* **43**, 3431-3456.

- [Reasor and Montgomery 2001] Reasor, P.D. and M. T. Montgomery, 2001: Three-dimensional alignment and corotation of weak, TC-like vortices via linear vortex Rossby waves, *J. Atmos. Sci.* **58**, 2306-2330.
- [Kossin and Schubert 2001] Kossin, J. P. and W. H. Schubert, 2001: Mesovortices, polygonal flow patterns, and rapid pressure falls in hurricane-like vortices, *J. Atmos. Sci.* **58**, 2196-2209.
- [Morikawa 1960] Morikawa, G. K., 1960, Journal of Meteorology **17**, 148-158.
- [Stewart 1943] H. J. Stewart, H. J., 1943, Q. Appl. Math. **1**, 262-267.
- [Willoughby and Black 1996] Willoughby, H. E. and P.G. Black, 1996: Hurricane Andrew in Florida: dynamics of a disaster, *Bull. Amer. Meteor. Soc.*, **77**, 543-549.
- [Wang and Wu 2004] Wang, Y. and C.-C. Wu, 2004: Current understanding of tropical cyclone structure and intensity changes - a review, *Meteorol. Atmos. Phys.* **87**, 257-278.
- [Fyfe 1976] Fyfe, D., D. Montgomery and G. Joyce, 1976: *J. Plasma Phys.* **17**, 369-.
- [Kraichnan and Montgomery 1980] Kraichnan, R. H., and D. Montgomery, 1980: *Rep. Prog. Phys.* **43**, 547-619.
- [Montgomey and Joyce 1974] Montgomery, D. and G. Joyce, 1974: *Phys. Fluids* **17**, 1139-.
- [Joyce and Montgomery 1973] Joyce, G. and D. Montgomery, 1973: *J. Plasma Phys.* **10**, 107-.
- [Montgomery et al. 1992] Montgomery, D., W.H. Matthaeus, W.T. Stribling, D. Martinez and S. Oughton, 1992: Relaxation in two-dimensions and the "sinh-Poisson" equation, *Phys. Fluids* **A4**, 3-6.

- [Spineanu and Vlad 2003] F. Spineanu and M. Vlad, 2003: Self-duality of the asymptotic relaxation states of fluids and plasmas, *Phys. Rev. E* **67**, 046309, 1-4.
- [Spineanu et al. 2004] Spineanu, F., M. Vlad, K. Itoh, H. Sanuki and S.-I. Itoh, 2004: Pole dynamics for the Flierl-Petviashvili equation and zonal flows, *Phys. Rev. Lett.* **93**, 025001, 1-4.
- [Nowak and Weimann 1990] Nowak, U. and L. Weimann, 1990: *GIANT* A software package for the numerical solution of very large systems of highly nonlinear equations, Konrad-Zuse-Zentrum fur Informationstechnik Berlin, Technical Report TR 90-11.
- [Deeam and Zabusky 1971] Deem, G. S. and N. J. Zabusky, 1971: Ergodic boundary in the numerical simulation of two-dimensional turbulence, *Phys. Rev. Lett.* **27**, 396-399.

This figure "fig\_4.jpg" is available in "jpg" format from:

<http://arxiv.org/ps/physics/0604059v1>